ELSEVIER

Journal of Structural Geology 27 (2005) 2204–2222

JOURNAL OF STRUCTURAL GEOLOGY

www.elsevier.com/locate/jsg

Geometry and growth of an inner rift fault pattern: the Kino Sogo Fault Belt, Turkana Rift (North Kenya)

William Vétel[a,*], Bernard Le Gall[a], John J. Walsh[b]

[a]*UMR-CNRS 6538 'Domaines Océaniques', Institut Universitaire Européen de la Mer, Place Nicolas Copernic, 29280 Plouzané, France*
[b]*Fault Analysis Group, Department of Geology, University College Dublin, Belfield, Dublin 4, Ireland*

Received 29 November 2004; received in revised form 21 June 2005; accepted 4 July 2005
Available online 16 September 2005

Abstract

A quantitative analysis is presented of the scaling properties of faults within the exceptionally well-exposed Kino Sogo Fault Belt (KSFB) from the eastern part of the 200-km-wide Turkana rift, Northern Kenya. The KSFB comprises a series of horsts and grabens within an arcuate 40-km-wide zone that dissects Miocene–Pliocene lavas overlying an earlier asymmetric fault block. The fault belt is ~150 km long and is bounded to the north and south by transverse (N50°E and N140°E) fault zones. An unusual feature of the fault system is that it accommodates very low strains (<1%) and since it is no older than 3 Ma, it could be characterised by extension rates and strain rates that are as low as ~0.1 mm/yr and 10^{-16} s^{-1}, respectively. Despite its immaturity, the fault system comprises segmented fault arrays with lengths of up to 40 km, with individual fault segments ranging up to ~9 km in length. Fault length distributions subscribe to a negative exponential scaling law, as opposed to the power law scaling typical of other fault systems. The relatively long faults and segments are, however, characterised by maximum throws of no more than 100 m, providing displacement/length ratios that are significantly below those of other fault systems. The under-displaced nature of the fault system is attributed to early stage rapid fault propagation possibly arising from reactivation of earlier underlying basement fabrics/faults or magmatic-related fractures. Combined with the structural control exercised by pre-existing transverse structures, the KSFB demonstrates the strong influence of older structures on rift fault system growth and the relatively rapid development of under-displaced fault geometries at low strains.

Keywords: Rift extension; Recent grid faults; Fault growth model; Remote sensing; Kino Sogo Fault Belt; Turkana Rift; Kenya

1. Introduction

In many continental rifts active deformation is focussed in a graben-like inner depression where syntectonic fluvio-lacustrine sediments accumulate, in association with extensive lava flows emitted from axial volcanoes. As a consequence, rift-related structures exposed on the floor of the inner trough are often partly or totally concealed beneath recent syn-rift cover, a factor that complicates any attempts to define fault system geometry. In these circumstances, numerous uncertainties arise concerning the geometry and kinematics of faults (nucleation, propagation and fault linkage) and even the calculation of bulk extension. Similar difficulties are often encountered in the axial trough of the East African Rift System (EARS hereafter) and along the eastern magmatic branch in Kenya, in particular (Fig. 1). The inner fault pattern of the Kenya Rift is, however, exceptionally well exposed in three specific areas (Fig. 1b), consisting of the Kino Sogo Fault Belt (KSFB) system, the Maji-Moto fault system and the Magadi fault system (Hackman et al., 1990; Le Turdu, 1998; Gloaguen, 2000). A common feature of these well-exposed fault systems is that they are developed within recent (<3 Ma) lava flows that are devoid of any overlying sedimentary deposits. Previous quantitative studies of the Maji-Moto and Magadi fault systems have provided improved definitions of either their extensional strain rate (Gloaguen, 2000) or their palaeo-stress fields (Le Turdu, 1998).

In this paper, we present a description and analysis of the geometry and growth of the KSFB using data constraints

* Corresponding author. Tel.: +33 2 98 49 87 41; fax: +33 2 98 49 87 60.
E-mail address: wvetel@univ-brest.fr (W. Vétel).

0191-8141/$ - see front matter © 2005 Elsevier Ltd. All rights reserved.
doi:10.1016/j.jsg.2005.07.003

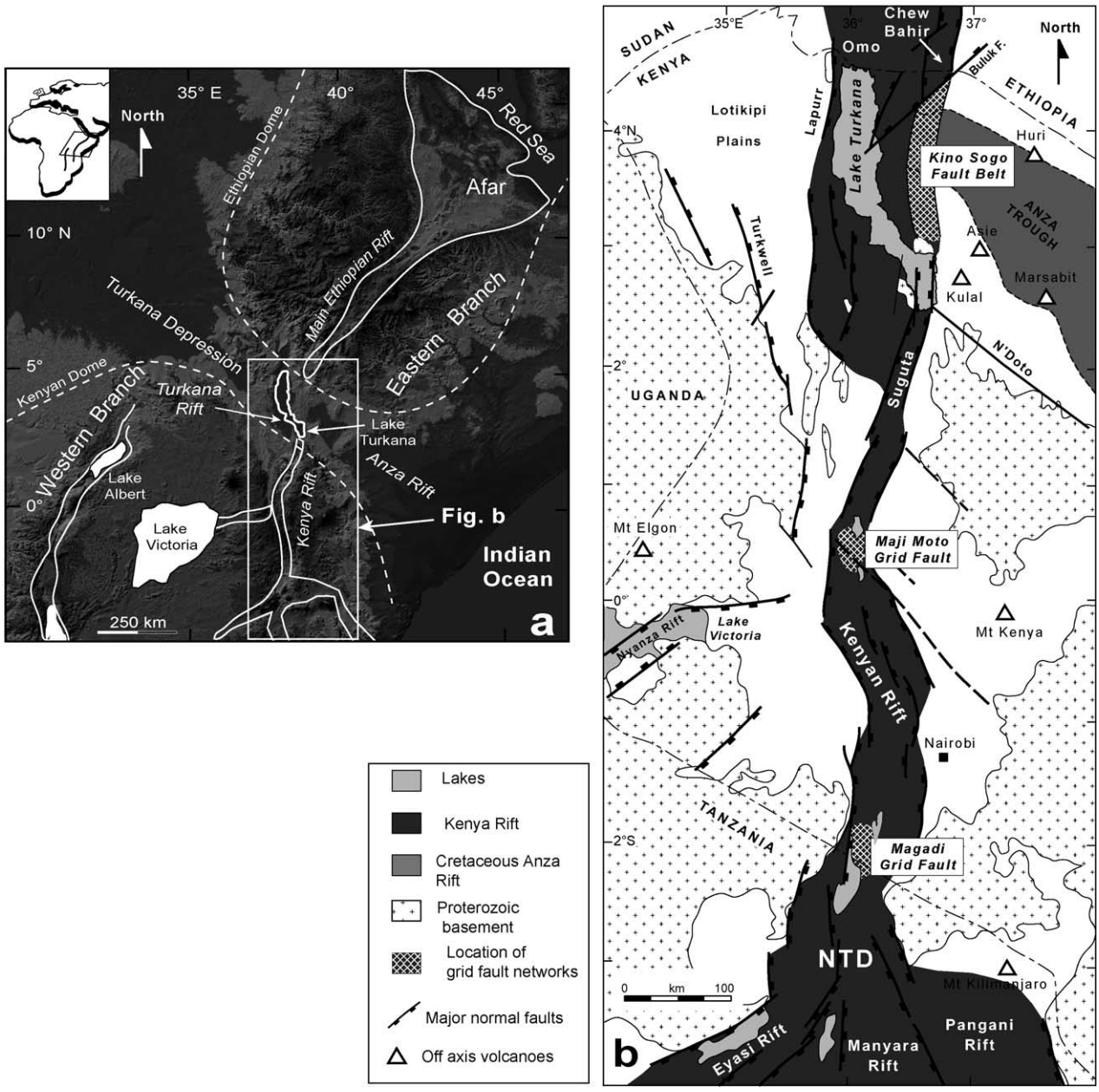

Fig. 1. General setting of the Turkana rift along the eastern branch of the East African Rift System (EARS). (a) Digital elevation model of the eastern part of the EARS (from Gtopo 30 data elevation data). The N140°E Turkana depression extends between the Ethiopian and Kenyan domes (dashed lines) following the trace of the Cretaceous Anza rift. (b) Structural map of the Kenya rift. Active deformation is concentrated along the linear and narrow Kenya trough except at its two extremities where the axial rift splits into three branches in the North Tanzanian divergence to the south and into a more subdued 200-km-wide rift zone along the Turkana area to the north. Inner-rift deformation is concealed by volcanics or sedimentary infill with the exception of three well exposed fault systems in the Kino Sogo (our study), Maji-Moto and Magadi areas.

derived from outcrop studies, remote sensing data and digital elevation models (Fig. 2). Quantitative analysis of the KSFB is greatly helped by the excellent definition of the fault system on the upper surface of Pliocene lava flows that are not disrupted by either younger volcanic edifices or later sediments. The fault system geometry accommodates only ~1% of fault-related extension during the past 3 Ma with potentially extremely low extension rates (0.1 mm/yr) and displays scaling properties, including displacement/length scaling and fault populations, which differ from those established from many fault systems characterised by higher strains (Schlische et al., 1996). We attribute these rift fault geometries and scaling properties either to the influence of structural inheritance from rift-parallel Proterozoic crystalline basement fabrics underlying the 200-m-thick Eocene–Pliocene lava pile and/or to the rejuvenation of a younger rift-related faults, the formation of which may have been partly controlled by a volcanic dome. The significance of earlier structures is

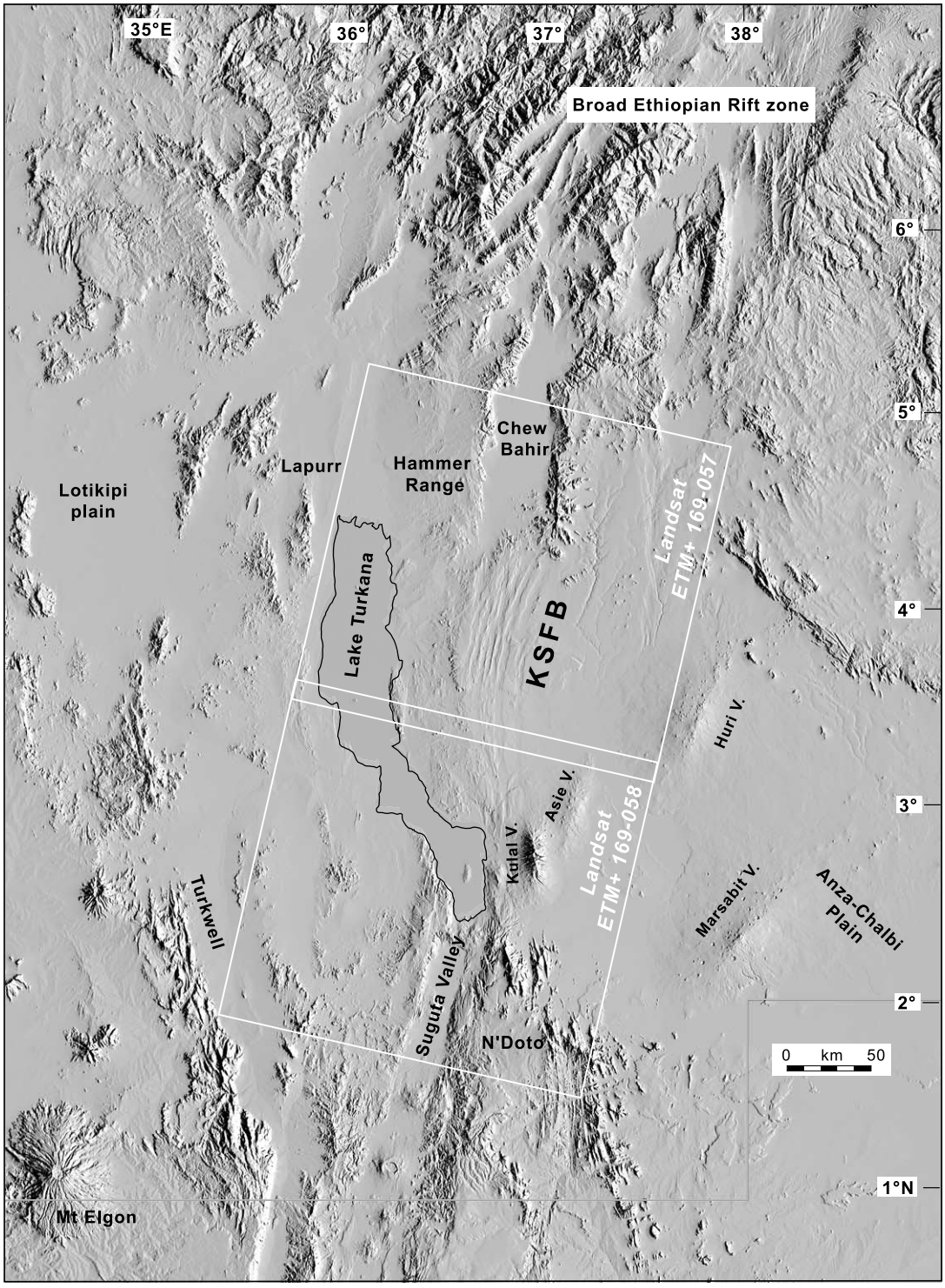

Fig. 2. Shuttle radar topography mission digital elevation model of the broad Turkana rifted zone (resolution 90 m in lateral, 16 m in vertical). White squares indicate the Landsat ETM+ coverage. Note the more subdued topography of the Turkana depression by contrast with Ethiopian and Kenyan relief to the north and south, respectively. The elevated Kino Sogo Fault Belt (KSFB) cuts through volcanics and is well-exposed relative to the adjoining depressed Chew Bahir graben, Suguta trough and Lake Turkana basin.

supported by the presence of cross-cutting, and possibly also contemporaneous faults, which parallel N50°E and N140°E oriented transverse discontinuities that bound the KSFB to the north and south, with the latter known to have controlled the formation of the Cretaceous–Palaeogene Anza Rift (Greene et al., 1991; Bosworth, 1992; Smith and Mosley, 1993; Dindi, 1994; Ring, 1994; Morley et al., 1999b; Vétel and Le Gall, in press).

2. Geological setting

Within the EARS, the Turkana depression is a polyphased rift system developed since Eocene–Oligocene times (~35 Ma; Dunkelman et al., 1989; Hendrie et al., 1994; Morley et al., 1999a; Vétel and Le Gall, in press). The KSFB is part of the youngest rift domain that mainly extends along the easternmost edge of the ~200-km-wide previously rifted zone (Figs. 1b and 2; Gabriel and Aronson, 1987; Ebinger et al., 1993, 2000). Because of the subdued and intricate topography of this eastern sector, typical rift morphologies are not easily recognised and a variety of contrasting models have been advanced for the spatio-temporal evolution of the rift. According to Dunkelman et al. (1988, 1989), the active zone of deformation is concentrated within the offshore basins of Lake Turkana and southwards into the linear, graben-like, trough of the Suguta valley (Bosworth and Maurin, 1993; Dunkley et al., 1993). In contrast, Hackman et al. (1990) proposed a double-armed rift system comprising the Lake Turkana faulted basins to the west and the KSFB into the Chew Bahir trough to the east (Gabriel and Aronson, 1987; Ebinger et al., 2000), with or without both arms linking southwards into the Suguta valley (Fig. 3). This model is favoured by our studies of both recent and earlier Cenozoic extensional fault patterns in the Turkana depression (Vétel and Le Gall, in press). Using new topographic and remote sensing datasets we also investigate the extent to which the N140°E Cretaceous Anza-type and N50°E structures of the Buluk Transverse Fault Zone (BTFZ) might have influenced the faulting process in the KSFB–Chew Bahir fault zones (Figs. 1 and 3).

Over the past ~35 Ma, the Kino Sogo area sensu lato was a dominantly volcanic domain comprising Eocene–Miocene lavas of the Balesa Koromto and Jarigole Fms in the west, overlain to the east by the Pliocene volcanics of the Gombe Fm. (north) and the Hurran Hurra Fm. (south) (Fig. 4; Charsley, 1987; Key and Watkins, 1988; Ochieng et al., 1988; Wilkinson, 1988; Haileab et al., 2004). This dominantly basaltic complex thins dramatically eastwards over an uplifted footwall block bounded by three major syn-magmatic extensional faults (Fig. 4b–d): (i) the N50°E-

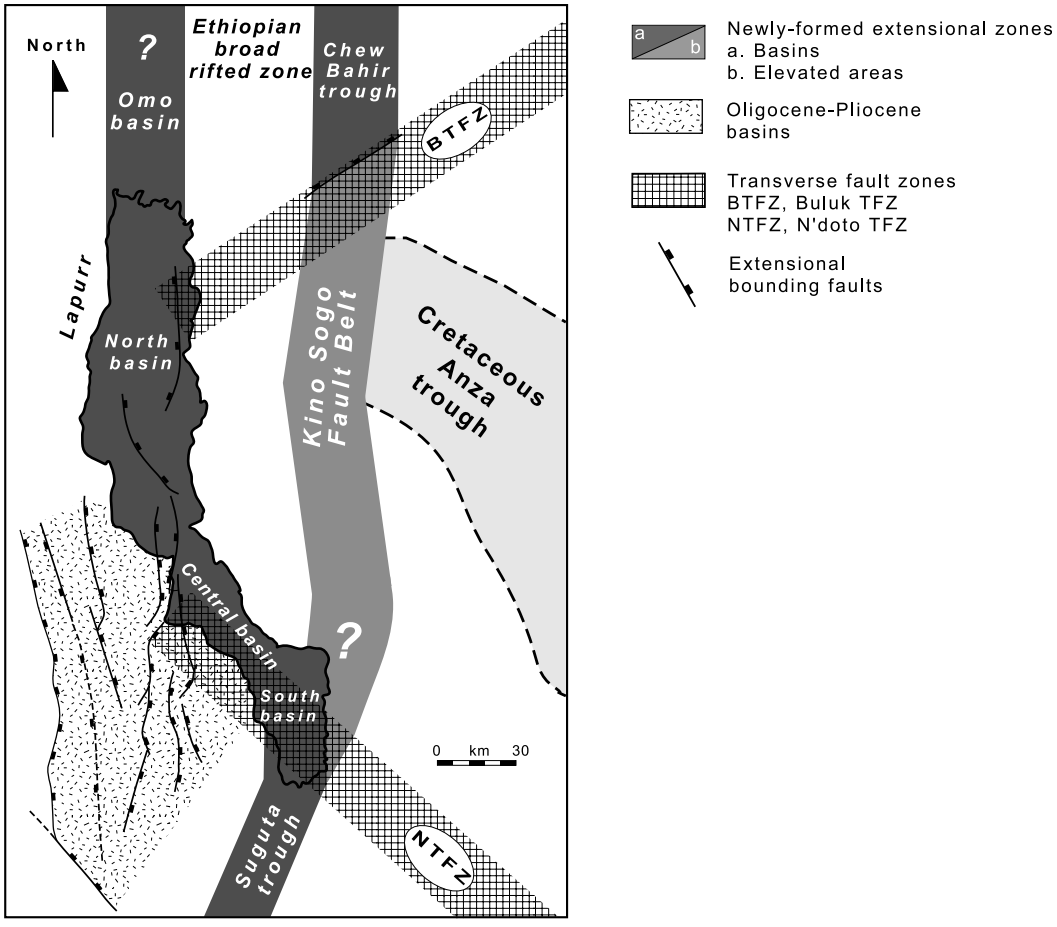

Fig. 3. Structural sketch map showing the location of recent/active deformation (<3 Ma) within the Turkana rifted zone. Note: (1) the existence of Oligocene–Pliocene deep half-grabens to the SW, not discussed in this work (Morley et al. (1999a) for further details); (2) the two parallel zones of recent deformation (Suguta, Lake Turkana basins, Kino Sogo and Chew Bahir) and; (3) the similar width of the two rift branches despite their contrasting structural styles.

trending Buluk Fault in the north, belonging to the 30-km-wide BTFZ, which displays an array of NE striking faults that partly accommodated the early development of the Chew Bahir basin during Miocene times (Vétel and Le Gall, in press); (ii) the Allia Bay fault (Fab) in the west, which is mainly documented from the rapid westerly sequence growth of the Eocene–Miocene Balesa Koromto/Jarigole Fms (Fig. 4c); and (iii) the Hoi fault in the east, which bounds the westernmost exposures of Miocene grits in the Anza basin (Fig. 4b; Morley et al., 1999b). During Eocene–Miocene times, the combined effect of these extensional faults led to the formation of an asymmetric horst block, with a general tilt to the SE (Figs. 4 and 5). This block is believed to have recorded significant internal extension along NS-trending fault structures that might have controlled the emplacement of Miocene intrusions such as the Jibisa volcanic complex to the NE (Hackman et al., 1990), adjacent to the transverse structures of the BTFZ (Fig. 4). The uplifted nature of the Kino Sogo fault block prior to the deposition of the Jarigole–Gombe volcanics is supported by the following lines of evidence: (i) the presence of a condensed, 250 m thick, Eocene–Pliocene volcanic sequence directly overlying basement; (ii) the rapid (six-fold) increase in thickness of this volcanic sequence to the west of the Allia Bay Fault (Fig. 4c); and (iii) the preservation of scattered inliers of Pliocene high-lake levels deposits of the Koobi Fora Fm. (Wilkinson, 1988; Feibel et al., 1989) within the Hurran Hurra region that represented a palaeo-embayment, south of the Kino Sogo area (Fig. 7b). Continued uplift of the Kino Sogo block following deposition of the Pliocene Gombe volcanics is defined by a gradual 200 m decline in terrain towards the east away from the Allia Bay Fault (cross-section 2 in Fig. 5). The KSFB post-dates and cuts through this tilted fault block into unexposed Proterozoic metamorphic rocks of the Mozambic belt at depth (Figs. 4 and 7; Smith and Mosley, 1993; Maurin and Guiraud, 1993; Shackelton, 1993; Hetzel and Strecker, 1994). Since the fault system cross-cuts Pliocene Gombe Fm. volcanics, it records deformation that is no older than $\sim$3 Ma (Hackman et al., 1990; Haileab et al., 2004). A younger age of faulting ($<$2.25 Ma) is possible assuming that the aligned intrusive bodies of the Kokurfo Bolol dated complex (Wilkinson, 1988) are controlled and dissected by the easternmost fault of the KSFB (Fe in Fig. 4b).

3. Morphology and geometry of the Kino Sogo Fault Belt

The geometry of the KSFB (Figs. 2 and 4) has been defined from satellite imagery (Landsat Enhanced Thematic Mapper Plus (ETM+)) and recently available topographic data (SRTM; shuttle radar topography mission; www.2.jpl.nasa.gov/srtm). The study area is covered by two Landsat ETM+ images (169–058, 23/10/1999 and 169–057, 27/01/2000). These images have been improved using Geomatica 9.2 and ENVI 4.1 softwares, by merging the panchromatic band 8 that displays the best ground resolution (unit pixel size of 15$\times$15 m) with spectrometric band 2 (green, 0.52–0.60 μm), band 4 (near infrared, 0.76–0.90 μm) and band 7 (middle infrared, 2.08–2.35 μm) images with lower ground resolution (unit pixel size 30$\times$30 m; Girard and Girard, 1999). These bands provide pixel reflectance and contrast that permit better constraints for the structural interpretation of satellite images. The digital elevation model has a lower lateral resolution (90$\times$90 m) but provides a 3D-visualisation of the fault system and definition of fault throws $>$16 m. Since numerous smaller faults, with throws $<$16 m, are resolved by the Landsat scene, the datasets are complementary together providing a more complete overview of the Kino Sogo fault system (Figs. 4 and 7). Apart from mapping the fault system, a variety of fault parameters (azimuth, length, spacing, throw) have been extracted from the 2D- and 3D-datasets as a prelude to our quantitative analysis of the fault system.

The KSFB is defined by a 40-km-wide system of extensional faults cross-cutting the pre-existing SE-dipping fault block (Figs. 4 and 5). In map-view, it forms a 150$\times$40 km arcuate fault system that is convex to the west and trends between N170°E, in the south, and N30°E, in the north (Figs. 4 and 7). It contains horst and graben structures bounded by two external inward-facing faults (Fw and Fe in Figs. 4 and 5). The easternmost fault (Fe) extends over the entire length of the fault system. Its southern trace, up to the middle part of the Gombe domain (i.e. the area defined by the Gombe volcanics), is composed of four NS–N10°E-oriented left-stepping fault segments, each $\sim$20 km long

Fig. 4. Geological and morphostructural context of the extensional Kino Sogo Fault Belt (KSFB). (a) Shaded shuttle radar topography mission (SRTM) digital elevation model of the Kino Sogo area (light from east and no vertical exaggeration). The location of sections in Fig. 5 is shown. (b) Structural interpretation of (a) from SRTM data of (same scale). The KSFB is subdivided into two distinct faulted areas, the Gombe highly faulted domain to the north and the Hurran Hurra apparently less deformed domain to the south. The Gombe domain is separated from the Chew Bahir trough to the north by the Buluk transverse (N50°E) fault zone (BTFZ). The first-order structures of the KSFB are dominated by a dense system of horst and graben controlled by normal faults that show variations in structural style along-strike. This system is bounded to the west and east by two inward-facing normal faults (Fw and Fe). Faults are disrupted in the Gombe domain showing numerous tips along the N120°E Central Transverse Fault Zone (CTFZ). (c) Rapid thickness variations in the volcanic cover from the Kino Sogo (section 2) westwards (section 1) via the Allia Bay extensional fault (Fab). (d) Structural sketch map of the KSFB showing the structural border faults of the Kino Sogo tilted fault block (Fab, Allia Bay fault; Fh, Hoi fault). The three segments of the Pliocene fault system ($<$3 Ma) are oriented from N170°E to N30°E northwards between left-stepping 'en échelon' border faults.

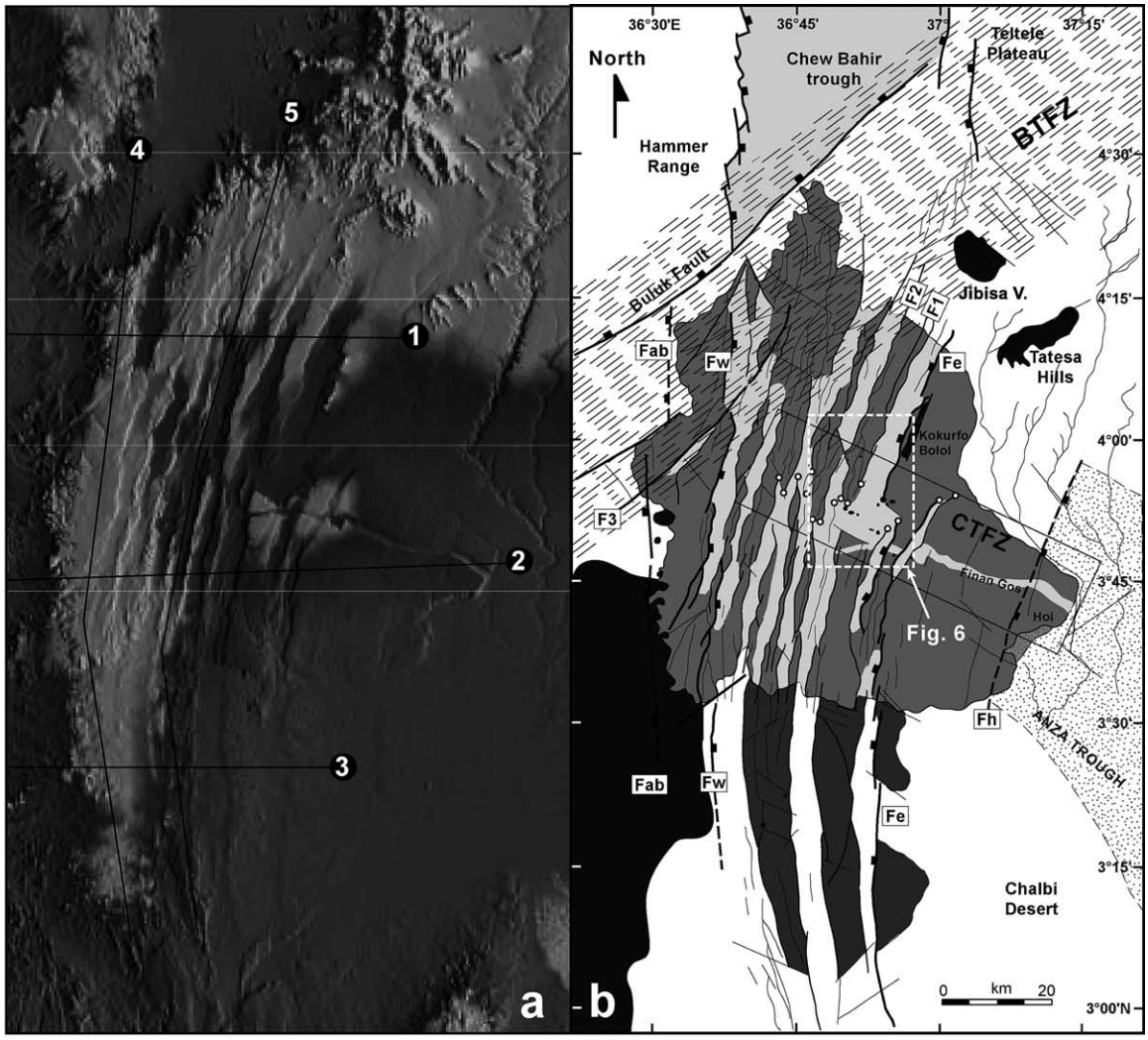
5
4
1
2
3
a
36°30'E
36°45'
37°
37°15'
North
Chew Bahir trough
Teltele Plateau
BTFZ
Hammer Range
4°30'
Buluk Fault
F2
F1
Jibisa V.
4°15'
Fab
Fw
Fe
Tatesa Hills
Kokurfo Bolol
4°00'
F3
CTFZ
Finan Gora
Hoi
3°45'
Fig. 6
Fh
ANZA TROUGH
3°30'
Fab
Fw
Fe
3°15'
Chalbi Desert
0 km 20
3°00'N
b

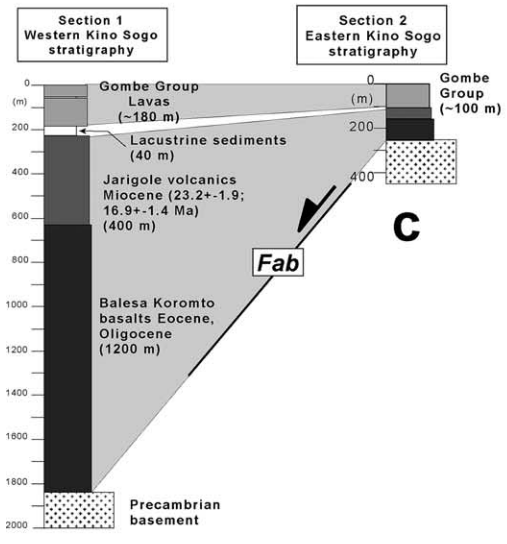
Section 1
Western Kino Sogo stratigraphy
Section 2
Eastern Kino Sogo stratigraphy
0
(m)
200
400
600
800
1000
1200
1400
1600
1800
2000
Gombe Group Lavas (~180 m)
Lacustrine sediments (40 m)
Jarigole volcanics Miocene (23.2+-1.9; 16.9+-1.4 Ma) (400 m)
Balesa Koromto basalts Eocene, Oligocene (1200 m)
Precambrian basement
Gombe Group (~100 m)
Fab
c

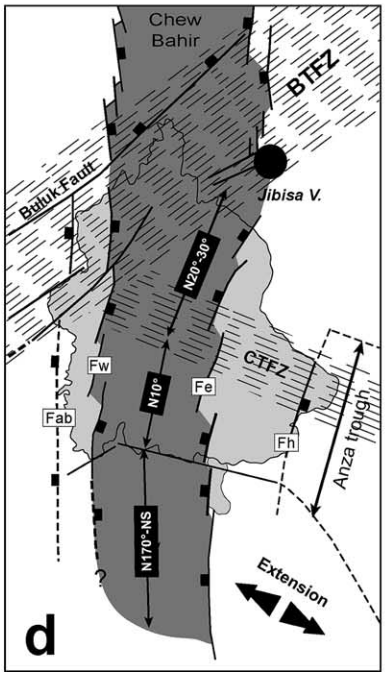
Chew Bahir
BTFZ
Buluk Fault
Jibisa V.
N20°-30°
Fw
Fe
CTFZ
N10°
Fab
Fh
Anza trough
N170°-NS
Extension
d

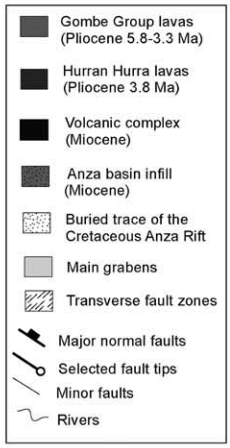
Gombe Group lavas (Pliocene 5.8-3.3 Ma)
Hurran Hurra lavas (Pliocene 3.8 Ma)
Volcanic complex (Miocene)
Anza basin infill (Miocene)
Buried trace of the Cretaceous Anza Rift
Main grabens
Transverse fault zones
Major normal faults
Selected fault tips
Minor faults
Rivers

(Fig. 4d). Further north, the trace of Fe is laterally offset by ~10 km to the west (and left) and then continues northwards as two almost co-linear and left-stepping, segments oriented at N20°–N30°E. 'En échelon' left-stepping fault segments also outline the trace of the western fault (Fw), which is, however, disrupted by Buluk-type transverse faults in the north. The southern extent of fault Fw is much less visible within the weathered Eocene–Miocene lavas. Indeed the southern part of the KSFB, north of the Kulal volcano and to the immediate W and NW of Asie volcano (Figs. 2 and 7), is poorly defined within the topographically subdued Hurran Hurra domain that is partly concealed by recent eolian sands and Eocene–Miocene lavas.

Structural sections across the fault system illustrate the gradual decline of the summit-level altitude towards the east, from 850 down to 600 m close to the Chalbi desert (Fig. 5). Along-strike (i.e. NS) sections show the elevated position (~800 m above sea level, on average) of the Gombe domain relative to the more subdued elevations (~600 m) of the Hurran Hurra and older basalts to the south. The Gombe domain gives way to lower elevation areas to the north and south across topographic scarps, approximately oriented at N50°E (north) and N120°E (south), and probably related to transverse faulting. This change in elevation is particularly clear on along-strike sections (see sections 4 and 5 in Fig. 5) crossing the boundary between the well-preserved highly faulted Gombe basalts to the north and the less well preserved and apparently less deformed terrain of the Hurran Hurra volcanics to the south.

The overall structure of the Gombe domain is dominated by a system of horsts and grabens bounded by first-order faults with maximum lengths of 35–40 km and vertical displacements that do not exceed 100 m (for example, F1 and F2 faults in Fig. 4b). In the north, the fault system comprises five pairs of N20°E-striking horst–graben with typical wavelengths of 8 km (see cross-section 1 in Fig. 5). The main bounding faults along the two easternmost horst–graben pairs are relatively continuous and linear, but are cross-cut and apparently offset by transverse (N50°E) faults of the ~30-km-wide BTFZ. The truncation and offset of individual graben across certain faults (e.g. F3 in Fig. 4b) are not, however, consistent, a feature that suggests that the transverse structures pre-date and are partly contemporaneous with the faults of the KSFB. In the south, the pronounced easterly tilted topography is cut by an increased number of horst–graben pairs (seven in cross-section 2 of Fig. 5) that are narrower than, and have strikes that are between 10 and 20° anticlockwise of, those in the north. The change from north to south appears to be defined by a 10-km-wide N120°E-trending depressed zone cutting across the central part of the Gombe domain (Figs. 4b and 6). On the radar DEM, numerous mapped faults appear to tip out within this zone, though closer inspection of the processed 2D-remote sensing data (lateral resolution of 15 m) reveals that some of the large faults splay into dense swarms of more segmented and smaller displacement faults within this zone (see F2 in Fig. 6). The resulting intricate fault patterns observed in this area evidently serve to allow southward transfer of fault-related strain onto a system with more, and therefore narrower, horst–graben pairs. This fault complexity is spatially associated with discrete N120°E-oriented discontinuities marked at the surface by a number of aligned circular intrusions (Figs. 4 and 6). These transverse faults may also extend 20 km further to the ESE along the linear course of the Finan Gos palaeoriver trace (Fig. 7b). Though the origin of this transverse zone of displacement transfer and complexity is unclear, its alignment sub-parallel to the earlier Cretaceous–Palaeogene Anza Rift would be consistent with some influence on the geometry of the Kino Sogo fault system by earlier reactivated cross-cutting structures. Further to the south within the Hurran Hurra basalts, most of the mapped faults are difficult to trace, though three of the horst–graben pairs are visible (cross-section 3 in Fig. 5). Despite the poor preservation of the fault system, the N170°E-striking faults are intensely disrupted by an array of N120°E faults (Anza-type) that occur as far north as the contact between Gombe and Hurran Hurra lavas (Fig. 7). These structures may also represent earlier reactivated faults associated with the southern margin of the Anza Rift.

4. Statistics of the Kino Sogo Fault Belt

Quantitative data for the Kino Sogo fault system have been derived for both the fault and fault segment populations defined from SRTM radar data and Landsat images (Figs. 2 and 7). The purpose of this analysis is to establish the basic scaling properties of the fault system as a means of testing a variety of models related to the geometry and kinematics of the system. Following a brief description of the methodology for defining individual faults and fault segments, orientation analysis is used to emphasize the importance of transverse faults, the presence of which is related to well-established earlier structures. We then use fault length population analysis to highlight the significant difference between this system and other fault systems, a feature that may reflect either the immaturity of the system and/or the role of inheritance from underlying structures. The spatial distributions of faults are presented for completeness, though their significance remains unclear. Displacement analysis, using available radar data, is then used to provide an estimate of the bulk extension, and limiting strain rates, across the system and to permit definition of fault displacement–length scaling, which is shown to be quite different from those of previously published fault systems. In our later discussion, we attempt to reconcile the unusual scaling characteristics of the KSFB with existing fault growth models.

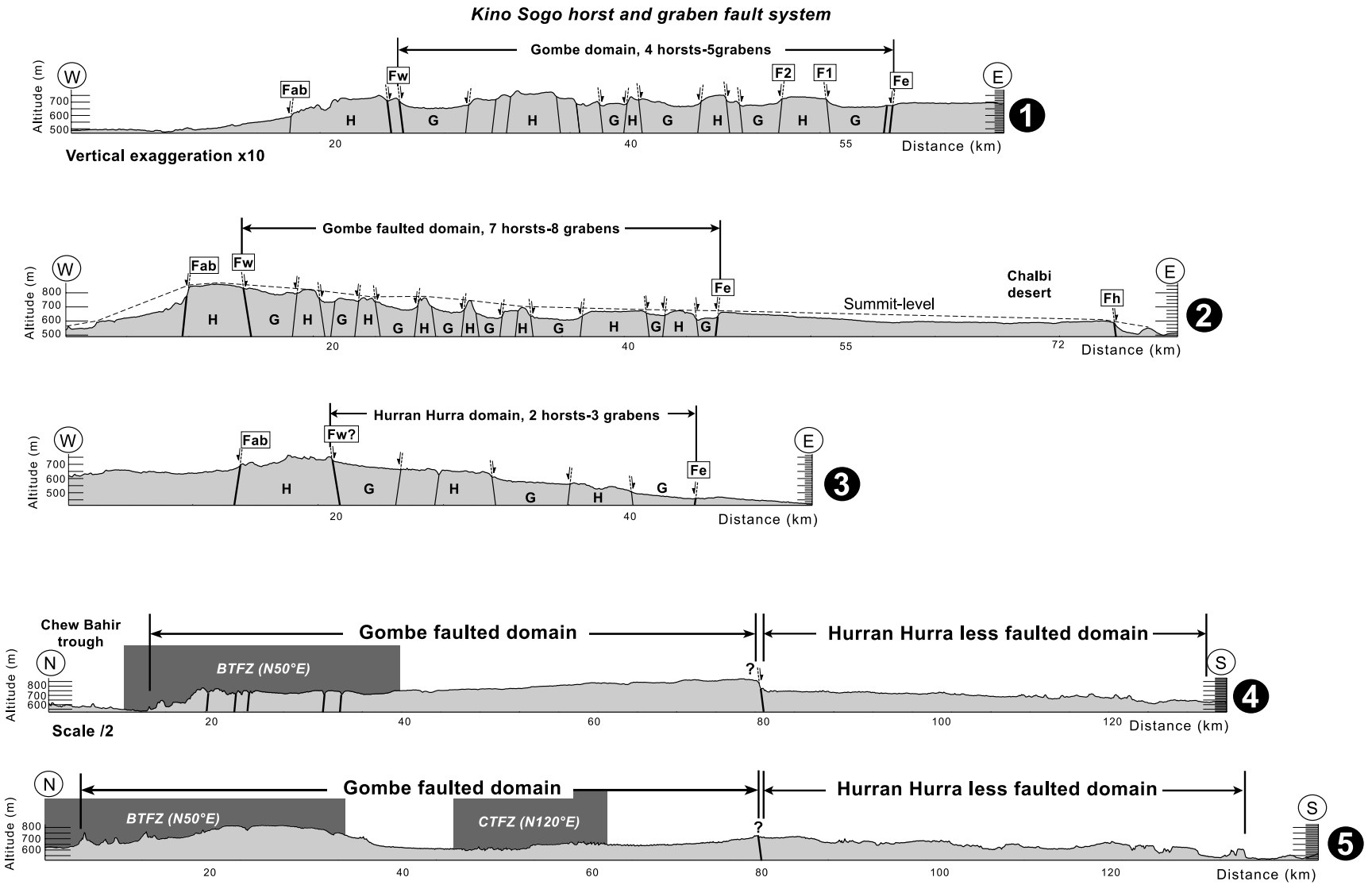

Fig. 5. Five structural sections across the Kino Sogo Fault Belt (vertical exaggeration ×10). Three across-strike sections (1, 2 and 3) and two along-strike sections (4 and 5) (see Fig. 4a for location). The sections highlight the along strike variations in structural style of the horst–graben system from the Gombe domain (sections 1 and 2) to the Hurran Hurra domain to the south (section 3). The summit-level line on section 2 shows the asymmetric morphology of the Kino Sogo-easterly tilted block. Along-strike sections 4 and 5 cut through two transverse faulted corridors (N50°E Buluk TFZ and N120°E Central TFZ) and the faulted boundary between the Gombe and Hurran Hurra domains.

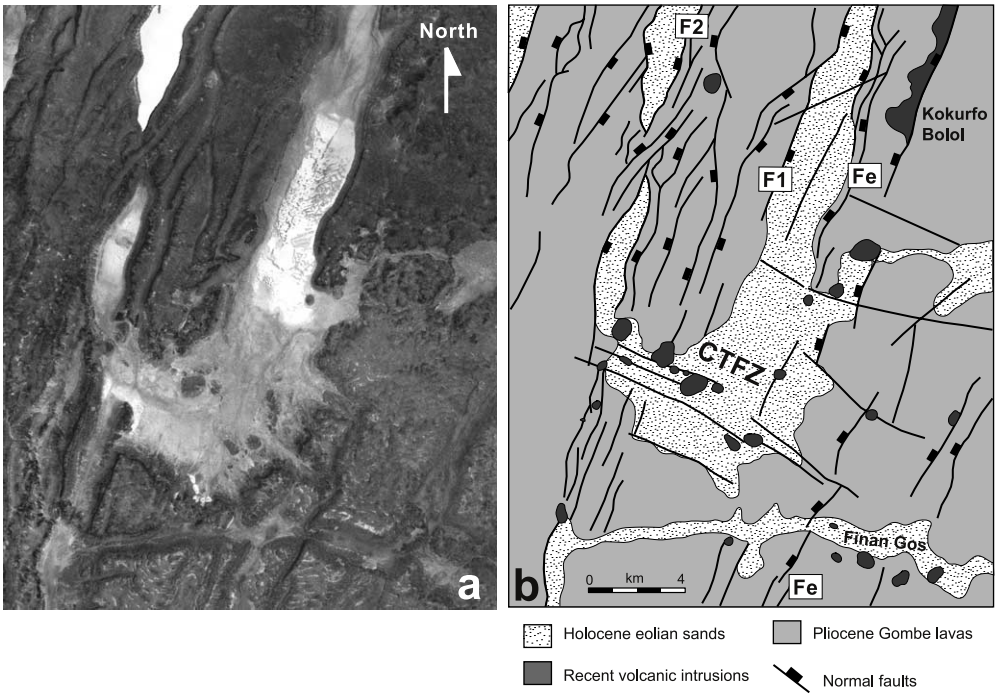

Fig. 6. Structural and magmatic expression of the N120°E-trending central transverse fault zone. (a) Detailed view of the Finan Gos area extracted from Landsat ETM+ satellite image. (b) Structural interpretation of (a) showing fault geometry complexities marked by: (1) a denser swarm of more segmented and smaller rift-parallel faults over the central transverse fault zone; (2) an approaching convergent transfer zone between two finger-like graben terminations and; (3) N120°E transverse trends outlined by faults and numerous recent volcanic intrusions.

4.1. Fault and fault segment sampling

Faults and fault segments were mapped from Landsat images with a lateral resolution of 15 m (Fig. 7). Individual fault segments were discriminated on the basis of the presence of fault tips, marked variations of fault azimuth or cross-cutting faults. Whether a fault segment is an element of a longer fault, or segmented fault array (Walsh et al., 2003), was determined on the basis of: (i) the presence of a relay zone with a narrow separation relative to fault segment length; (ii) equivalence of throw and downthrow direction between segments; and (iii) similarity of footwall dips on adjacent segments (Peacock and Sanderson, 1991; Cartwright et al., 1995; Cardon, 1999; Gloaguen, 2000; Walsh et al., 2003). A total of 427 individual faults were identified in the Gombe and Hurran Hurra domains, with 1718 fault segments. The high ratio of segments to faults (4/1) reflects the highly segmented nature of the entire fault system, as evidenced by the segmented bounding faults in particular (Fe and Fw in Fig. 4). The preservation of relay zones is not, however, surprising given the low displacements on individual segments and the relatively high overlap lengths and separations of many relays. Along the southern portion of the eastern bounding fault (Fe), for example, overlap lengths in excess of 2 km are developed between five successive segments with 100 m throw, geometries that require relay ramp gradients of less than 1/20, i.e. 3° ramp dip, values that are within the range of typical intact relay ramps (Imber et al., 2004). Later, we suggest that this highly segmented fault system is partly attributable to the very low displacements, and therefore strains, accommodated by the system.

4.2. Fault and segment-trace orientations

The orientation distributions of the faults and fault segments of the Gombe and Hurran Hurra domains are presented in Fig. 8. These plots highlight the presence of three distinct trends. The dominant faults are N350–30°E-striking structures corresponding to the general trend of the Cenozoic rift. Two other distinct secondary trends correspond to the N50°E and N140°E faults of the BTFZ and Anza rift, respectively. As discussed earlier, the latter are best seen in the Hurran Hurra domain to the south, where they generally correspond with the lateral extension of the Anza rift, whilst the former are widely developed in the Gombe domain to the north and arise from the cross-cutting BTFZ. Although these relationships reinforce the notion that earlier structures have influenced, to some extent, the geometry of the fault system, much of the central Gombe domain is relatively unaffected apart from the possible central transverse structure (Anza-type), already referred to, which appears to be responsible for enhanced fault and horst–graben segmentation.

4.3. Length of fault and fault segment

In this section, the fault and segment length statistics are presented for the main rift-parallel faults (N350–30°E) of

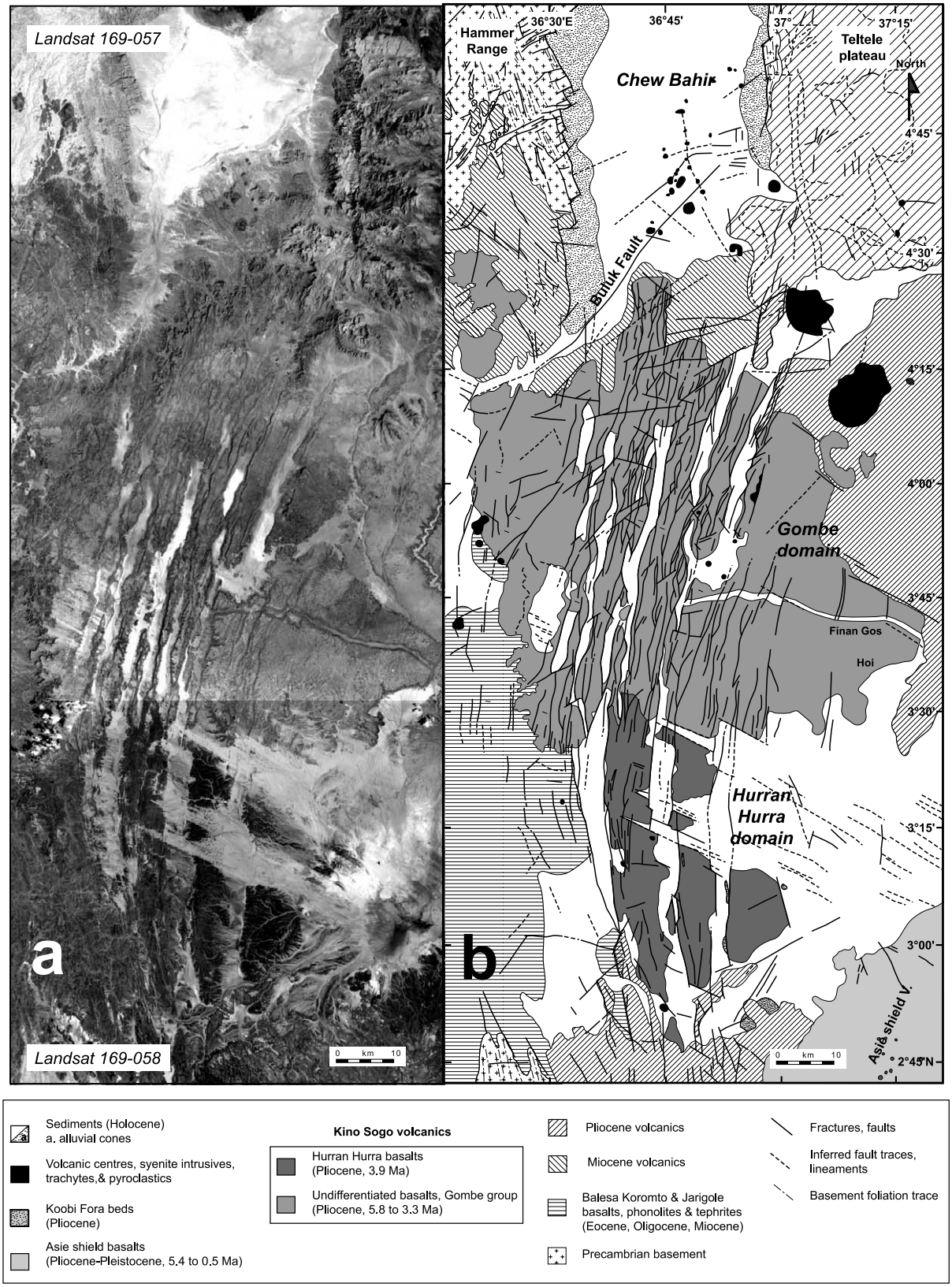

Fig. 7. Structural map of the Kino Sogo Fault Belt (KSFB). (a) Detailed view of the KSFB extracted from Landsat ETM+ processed satellite image. (b) Structural interpretation of (a). The map highlights the structural contrast between the Gombe and the Hurran Hurra faulted domains.

the Kino Sogo fault system. Emphasis is placed on characteristics of the better exposed faults and fault segments of the Gombe domain, for which rift-parallel faults are far more numerous and longer than other trending structures (Table 1). The Hurran Hurra domain data are likely to be strongly biased by poorer exposure and partial burial by eolian sands. Histograms of fault and segment length show a marked decrease in the frequency of faults and segments with lengths below 5 and 2 km, respectively; values that are much greater than the lateral resolution of the Landsat images (>15 m) (Fig. 9a and b). Because our comparison of the Landsat and radar fault maps suggests that the Landsat map contains faults that are significantly below the vertical resolution of available digital elevation models (≪16 m), it is unlikely that the decrease in fault frequency is a function of fault throw resolution. The frequency distributions therefore suggest that there is a real decrease in the frequency of short faults and segments, a feature that is not consistent with the often described fractal nature (self-similar) of other fault systems (Main, 1996; Yielding et al., 1996; Cardon, 1999).

The scaling properties of length populations are explored further using conventional cumulative frequency versus length distributions, which plot the cumulative number of faults or segments (N) with lengths greater than a given value (L). When plotted in log–log and linear–log space, this type of plot permits identification of different types of distribution, in particular power-law and exponential. Exponential relationships provide straight-line distributions in linear-log plots and are defined by:

$$N(L) = \alpha e^{-\lambda L} \tag{1}$$

where N is the number of faults, or segments, with length greater than or equal to L, α is the total number of measures and λ is a scale parameter.

Power-law relationships provide straight-line distributions on log–log plots and are defined by:

$$N(L) = \alpha L^{-C} \tag{2}$$

where N is the number of faults, or segments, with length greater than or equal to L, α is a constant and C is the

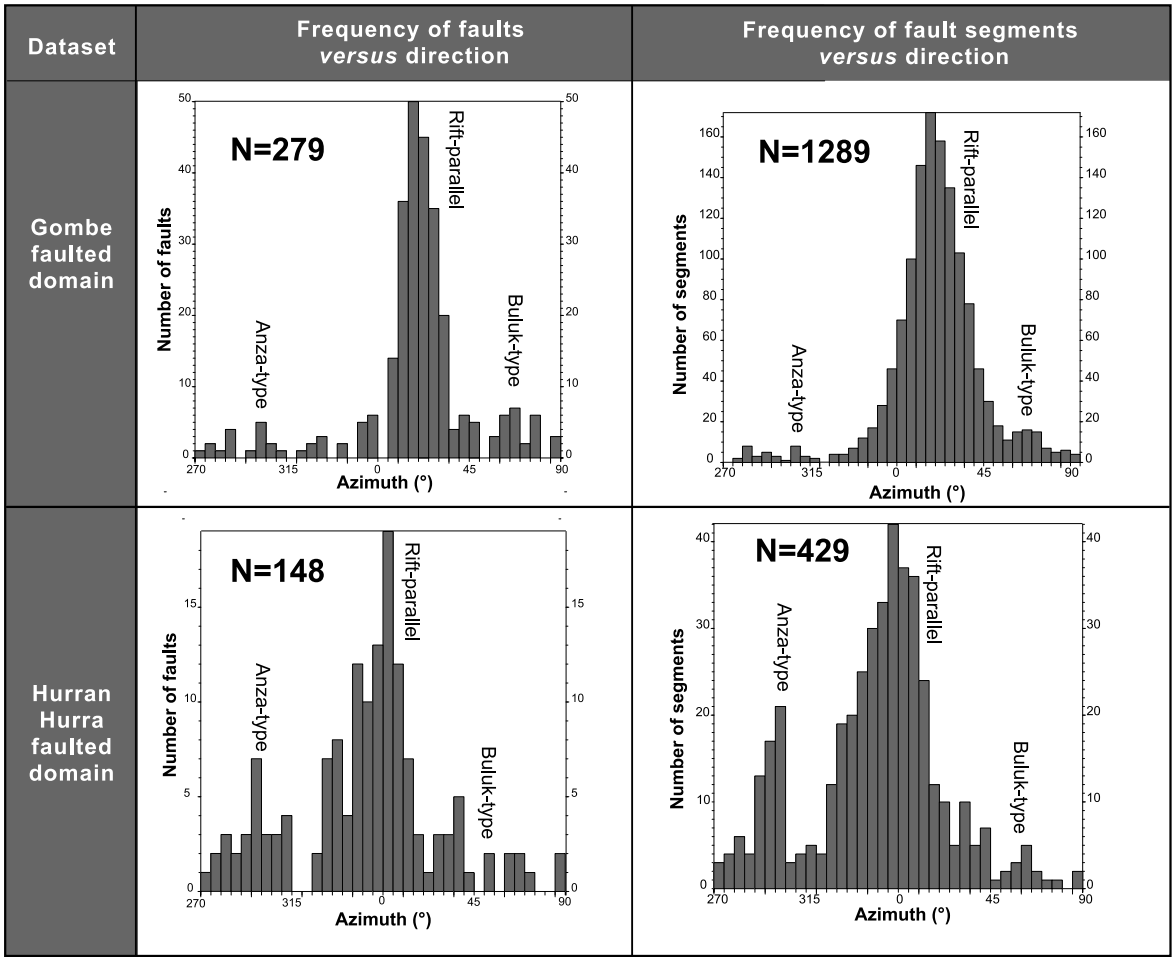

Fig. 8. Histograms illustrating the frequency of faults and fault segments versus direction in the Gombe and Hurran Hurra domains. The three main directions of structures are the dominant N350–N30°E rift-parallel faults and two subsidiary N50°E (Buluk-type) and N140°E (Anza-type) transverse features. The data indicate a swing of fault azimuths from N170°E to N30°E northwards.

Table 1
Principal statistical parameters of the lengths of Gombe and Hurran Hurra faults and fault segments

	NS–N30° Rift-parallel	N40°–60° Buluk-type	N120°–140° Anza-type	NS–N30° Rift-parallel	N40°–60° Buluk-type	N120°–140° Anza-type
Gombe fault length (L)				Gombe fault segment length (L)		
Number	211	16	10	930	74	14
L max (km)	37	24	20	14	24	10.5
Cumulative L	2046	244	75	1964	240	70
Mean L	9.7	7	6.5	2	3.3	5.4
Hurran Hurra fault length (L)				Hurran Hurra fault segment length (L)		
Number	45	5	12	127	13	35
L max (km)	35	11.4	26	8	4.5	25
Cumulative L	347	34	85	342	42	167
Mean L	7.7	6.8	4	2.7	3.2	4.8

power-law exponent. Examination of both fault length and segment length populations for the Gombe domain suggests that the Kino Sogo fault system does not ascribe to the power-law, or fractal, nature of fault populations displayed by many other fault systems (Fig. 9c and d; Childs et al., 1990; Scholz and Cowie, 1990; Walsh et al., 1991; Nicol et al., 1996; Yielding et al., 1996). Not only do the population distributions on log–log plots provide non-linear curves, which cannot be attributed to sampling issues such as truncation at small lengths or censoring at large lengths (because fault lengths are much shorter than the length of the study area), potential straight line portions of the distributions (between 10 and 30 km fault length) have excessively high exponents (i.e. significantly higher than the usual 1–2 range from other fault systems; see Cladouhos and Marrett, 1996). By contrast, the length populations are much more consistent with an exponential distribution (Fig. 9e and f), which is rarely described but has previously been attributed to either the early initiation phase of fault system evolution, when the initiation of new small faults dominates the growth of existing faults, or the final phase of mature fault system evolution when large faults cut through the brittle layer thickness and the system progressively becomes saturated (Villemin and Sunwoo, 1987; Cowie et al., 1995; Ackermann and Schlische, 1997; Ackermann et al., 2001; Spyropoulos et al., 2002). Whilst the relatively low strains associated with the Kino Sogo fault system (see below) may be consistent with an early growth stage, the very long fault lengths observed in the area would generally be taken as an indicator of fault system maturity. This apparent conflict is returned to in a later section.

4.4. Fault spacing

The best indication of the spatial distribution of the Kino Sogo fault system is the relatively consistent spacing of horst–graben pairs along fault-perpendicular sections (Figs. 4 and 5). Fault maps indicate an increase in the number of horst–graben pairs in the south, with a corresponding decrease in spacing, the origin of which is unclear. For completeness, however, 162 fault spacings have been measured between adjacent rift-parallel faults on five ~EW cross-sections (15 km apart) in the Gombe domain. Plots of fault spacing versus cumulative frequency are characteristic of an exponential-law model rather than a power-law model (Fig. 10). Taken together, the relatively systematic spacing of horst–graben pairs and the exponential spacing distributions, suggest the presence of some dominating km-scale structural control complicated by randomly distributed smaller faults. Although other studies elsewhere have suggested that regular large-scale fault spacings could be related to the thickness of a faulted layer or crustal thickness (Wu and Pollard, 1995; Ackermann et al., 2001; Spyropoulos et al., 2002), this explanation is not easily applied to the Kino Sogo system.

4.5. Maximum fault displacements

The maximum throws of 30 of the larger faults within the Gombe domain have been derived from the topographic elevations along fault scarps resolved by the SRTM dataset (16 m vertical resolution). For each fault, vertical throws were measured at approximately 5 km intervals along the lengths of their fault scarps. The range of maximum throw is between 30 and 100 m for faults that are between 9 and 36 km in length (Fig. 11); throws as low as 16 m have been measured but maximum throws are typically >30 m. Although the range of fault throws and lengths is relatively narrow, faults from the Kino Sogo system show a weak positive correlation between displacement and length. Similar positive relationships between fault length and displacement have been established by numerous previous studies and have underpinned the development of different fault growth models in which the maximum displacement (D) of faults scales with fault length (L), following the expression:

$$D = cL^n \tag{3}$$

where c is a constant and n is between 1 and 2 (Walsh and

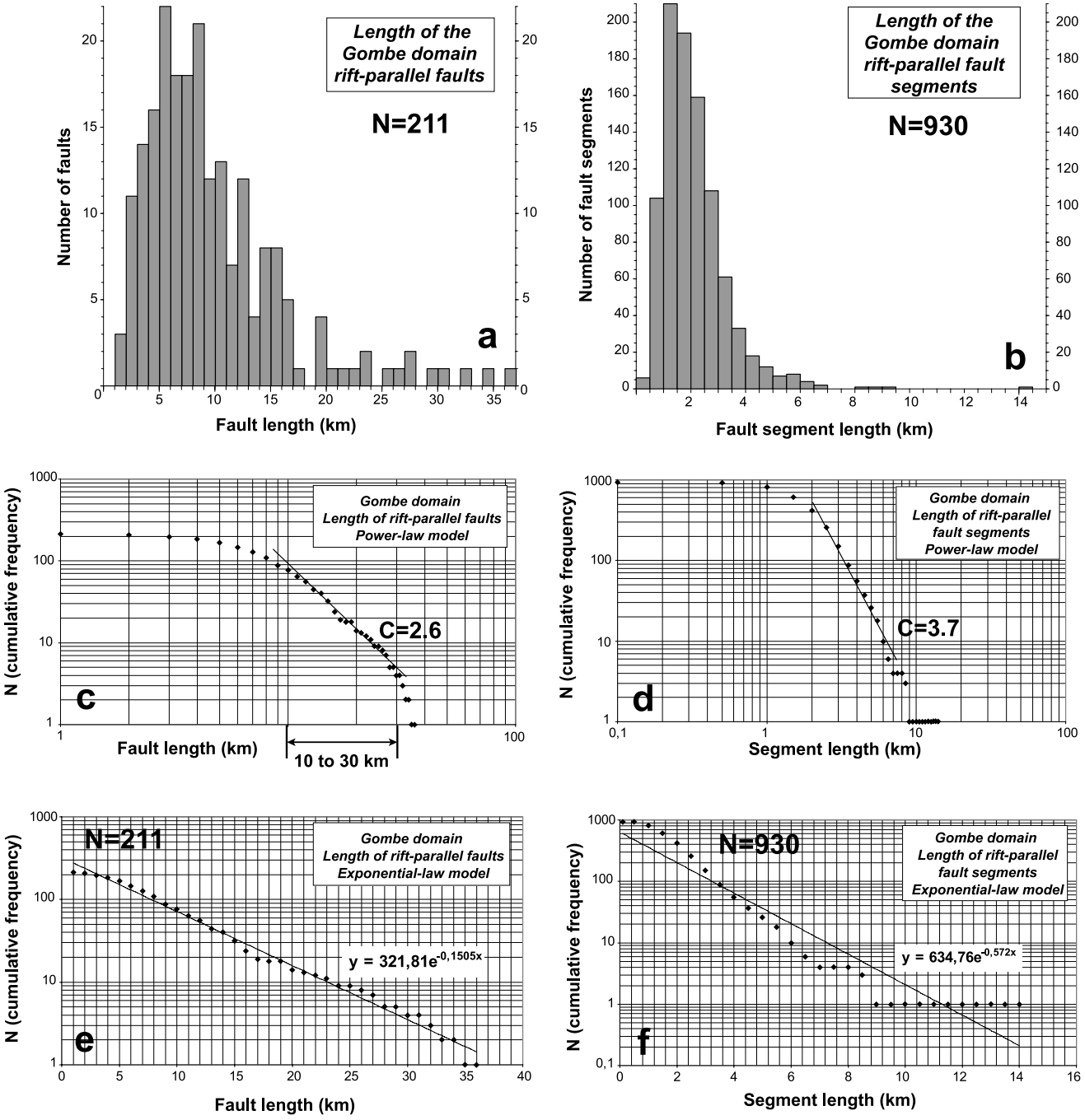

Fig. 9. Distribution of rift-parallel faults and fault segment populations in the Gombe domain. (a) and (b) Frequency of rift-parallel faults (each km) and fault segments (each 500 m) versus length. The decrease in frequency of faults <5 km and fault segments <2 km is not due to censoring effects. (c)–(f) Cumulative frequency plot of rift-parallel structures versus length and fit with statistic law models. (c) and (d) Log–log cumulative frequency plots of faults and fault segments versus length showing a poor fit with a power-law distribution. Left- and right-hand truncations are not due to undersampling and area-scale effects. The slope of $C=2.6$ is calculated for the central segment of the length curve between 10 and 30 km. (e) and (f) Log–linear cumulative frequency plots of faults and fault segments versus length showing a good fit with an exponential distribution.

Watterson, 1988; Cowie and Scholz, 1992; Gillespie et al., 1992; Dawers et al., 1993; Schlische et al., 1996). The scaling law (3) is generally taken to be a growth trend and underpins fault growth models involving a sympathetic increase in both the lengths and maximum displacements of faults as the fault system evolves (Walsh and Watterson, 1988; Cowie and Scholz, 1992). The distinctive feature of the Kino Sogo fault system is that although it provides a weak positive correlation between fault displacement and length, it defines a field that falls well below other fault systems, so that faults of a given length are significantly under-displaced (Fig. 11). Before considering the

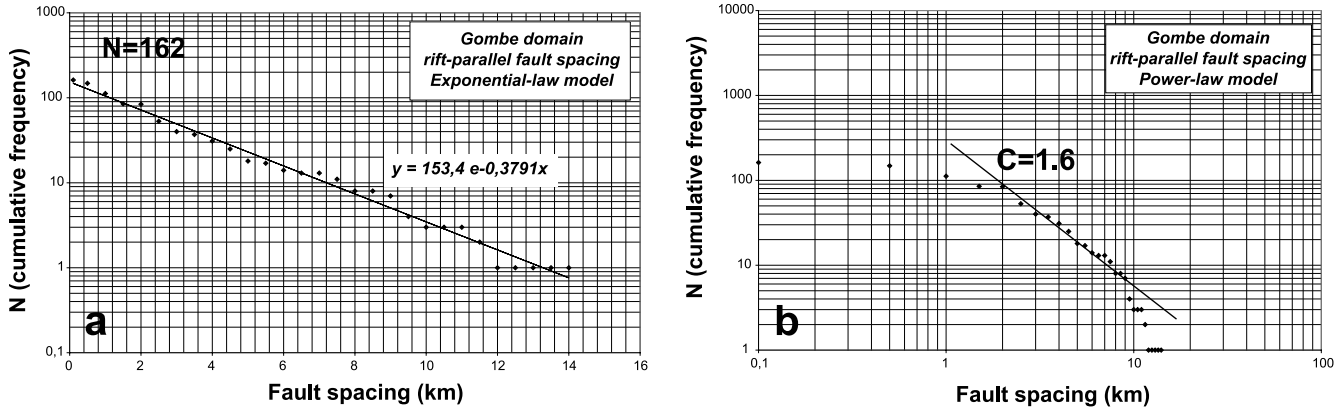

Fig. 10. Log–linear (a) and log–log (b) cumulative frequency plot of rift-parallel fault spacing in the Gombe domain. Spacing data best correlates with an exponential distribution.

significance of this feature, we first derive estimates for the bulk extension and strain rates associated with the Kino Sogo fault system.

5. Rift extension and strain rate

The cumulative fault-related extension has been calculated directly from the available SRTM data using the following procedure. First, aggregate throw is calculated from the measured throws at the intersection points of all faults with four regularly spaced E–W sections across the fault system. The average cumulative throw for the 40-km-long cross-sections is then used to compute the cumulative heave for a range of plausible fault dips. Fault dips cannot be directly measured from SRTM data but previous studies in the Kenya rift suggest average fault dips in the range 60–70° (Walsh and Watterson, 1988; Le Turdu, 1998;

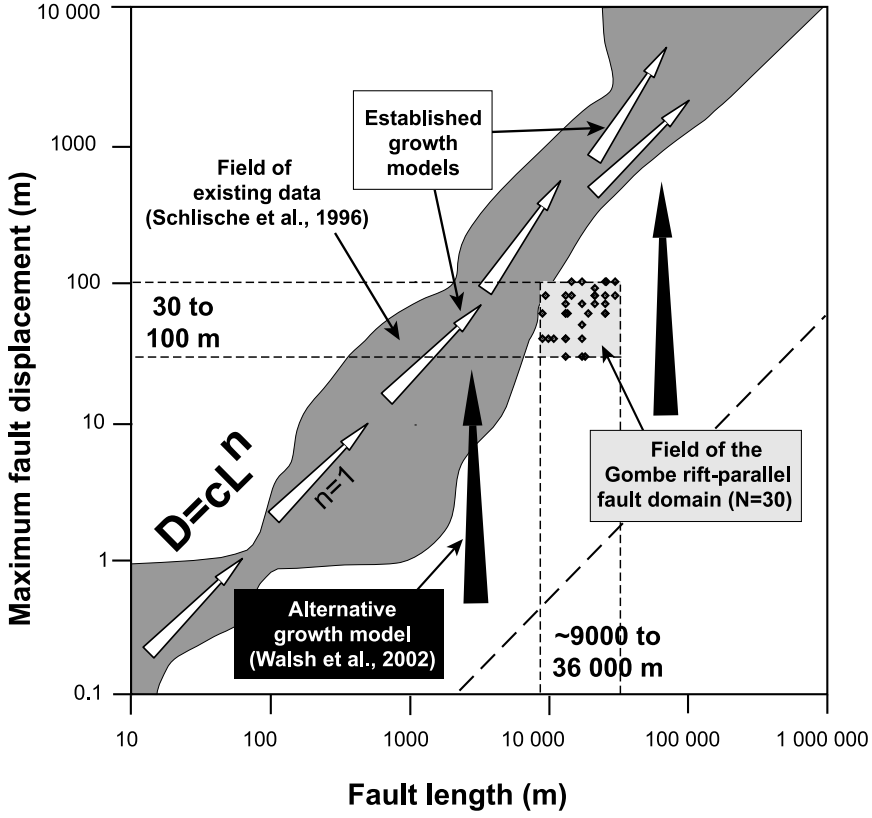

Fig. 11. Log–log plot of maximum fault displacement versus length showing the 'under-displaced' nature of the rift-parallel normal faults in the Gombe domain relative to published fault data (Schlische et al., 1996) and growth paths of faults predicted by conventional models (white arrows). By contrast, the Kino Sogo fault data are in agreement with an alternative fault growth model (Walsh et al., 2002) (black arrows) in which fault lengths are established from an early stage and fault growth is dominated by displacement accumulation.

Gloaguen, 2000). The cumulative fault throw and fault dips combine to provide cumulative heaves of between 450 and 285 m for the 40-km-wide rift. These heave estimates correspond to extension values between 1.1 and 0.7% and stretching factors (β) between 1.01 and 1.007, values that are much lower than the 3–8% extension in the axial trough of the Kenya rift (Gloaguen, 2000) and the 12% extension estimate in the Afar rift (Gupta and Scholz, 2000) (see Fig. 1). These values are also much lower than those described for other rifts, which are often characterised by stretching factors greater than 1.1 (e.g. the Jeanne d'Arc Basin, Grand Banks and Viking Graben; Kusznir et al., 1991). Therefore, even accounting for the possible contribution of faults with throws less than 16 m, the strains associated with the KSFB are nearly an order of magnitude lower than those of typical rifts, a feature that has profound implications for the growth of the fault system (see below).

Estimates of rift extension rates and regional strain rates require definition of the entire period of faulting. The 3 Ma age of the host lavas defines an upper limit to the possible period of activity and associated minimum estimates of both extension rate (0.15–0.095 mm/yr) and strain rate (1.16×10^{-16}–7.4×10^{-17}). It is not possible, however, to estimate a lower limit for the period of fault activity though regional considerations suggest that the fault system was active for recent periods (Holocene?). The extended period of fault activity (3 Ma to Present) provides estimates of extension rate that are a small fraction of the 1–4 mm/yr extension rate estimates for the adjacent Kenyan or Ethiopian rifts over the period from Pliocene to Present (Morley et al., 1999a; Ebinger et al., 2000; Gloaguen, 2000). Assuming similar rates applied to the multi-rift Turkana zone, then if the KSFB were at any time to have been the sole active component of the zone, it could not have been active for more than ~300,000 years. To reconcile our estimate of the KSFB deformation rates and those of the Turkana rift zone therefore requires that it was either active continuously at very low strain rates concomitantly with offshore Lake Turkana basins further west (see Fig. 3) or that it had a short-lived history (~300,000 years) within that 3 Ma-long period. Although we cannot yet define the period of fault activity, the most significant issue for the purposes of this article is that the fault system is characterised by very low strains.

6. Discussion

One of the most distinctive features of the Kino Sogo fault system is the very low (~1%) extension recorded across the 40-km-wide rift. Such very low strains potentially may also provide a rationale for other characteristic features of the fault system including: (1) the under-displaced nature of individual faults; (2) the highly segmented nature of the fault system; and (3) the fault size scaling properties. Displacement–length data for the KSFB define a field below that occupied by conventional fault growth trends and indicating relatively low displacement/length ratios (Fig. 11). Their under-displaced nature is, however, consistent with an alternative fault growth model, described by Walsh et al. (2002), in which fault lengths are established during rapid early stage fault propagation, followed by a more protracted period of displacement accumulation with retarded fault propagation arising from interaction between adjacent faults. The earliest phases of growth are therefore characterised by under-displaced faults, which grow into conventional 'growth' trends rather than along them (Fig. 11). Walsh et al. (2002) showed that a fault system in the Timor Sea characterised by fault-related extension of ~3% now shows displacement/length scaling within the general field for other fault systems, but that early stage fault growth was characterised by lower displacement/length ratios. Their model would therefore predict that fault systems with very low extensions of ~1%, similar to those estimated for the KSFB, should have under-displaced faults. This prediction is consistent with both the strongly segmented geometry of the Kino Sogo faults and their under-displaced nature. Further displacement accumulation would be expected to result in progressive relay breaching and map-view linkage of fault segments with progressively larger separations and overlap lengths (Imber et al., 2004). The relatively small separations between adjacent fault segments and the displacement conservation along their combined lengths suggest that individual segments may even link at depth, in which case later map-view linkage would change the fault map but would otherwise have a limited impact on fault growth (Walsh et al., 2003).

Although rapid fault propagation within the Timor Sea fault system in the past 6 Ma has been attributed to the reactivation of pre-existing, and underlying, Jurassic normal faults, Walsh et al. (2002) suggest that rapid early stage fault propagation may be typical of fault systems that have developed ab initio. The rapid generation of fault lengths, with a broad range of size, contrasts with conventional fault growth models in which the nucleation of smaller faults is followed by the progressive increase in both the length and displacement of some faults. No direct observational constraints favour either the conventional or alternative fault model in previously unfaulted volumes. The potential influence of earlier structures cannot, however, be ruled out in the case of the KSFB, where there are at least three types of pre-existing structures that could be responsible for the rapid fault propagation and the 'under-displaced' nature of faults (Fig. 12):

(i) Ductile basement foliation planes, showing a N170°E–N30°E sigmoid structural grain, are clearly visible within the N'Doto Proterozoic basement massif, which occurs to the south of the KSFB (Fig. 12a and b). The arcuate trace (convex to the west) of the Kino Sogo fault grid displays a quite similar wavelength (~200 km) as those of the

basement strain trajectory (convex to the east) in the N'Doto massif. Taking into account the Hammer Range to the north, the basement pattern in the Turkana rift as a whole is seen to involve a sinusoidal-shaped fabrics dissected by nearly orthogonal (N50°E and N140°E) transverse fault zones at the inflection points (Fig. 12b). It is possible, therefore, that the rift fault system in the KSFB could have been promoted by the existence of curved underlying Precambrian basement fabrics.

(ii) Proterozoic, and perhaps even rift-related, faults might have existed within the basement rocks underlying the faulted Gombe lavas, but their existence is not easily demonstrated because they would have been subsequently eroded on the uplifted flanks of the Allia Bay fault (Fab) to provide an apparently unfaulted surface upon which the lavas were deposited. It is possible, nevertheless, that at some time prior to 3 Ma, a fault system may have existed along the KSFB and could therefore have linked the Chew Bahir trough, in the north, to the Suguta trough, in the south.

(iii) Earlier faults/fractures may have developed in association with bending stresses related with thermally induced domes that have been inferred to have formed in the Kino Sogo volcanic area during two successive volcanic events at 35–12 and 6–3 Ma (Watkins, 1986) (Fig. 12b–d). Under WNW–ESE extension, these faults would have been NNE-oriented and could therefore have subsequently guided the propagation of extension throughout the Kino Sogo domain during the deflation phase following the Pliocene volcanic/doming activity. Similar dome/faulting interactions have been interpreted for the western part of the Turkana rift during Miocene times (Vétel and Le Gall, in press).

To summarise, the existence of earlier fabrics and faults within the basement would, on their own, provide a rationale explanation, not only for rapid fault propagation within the Gombe lavas, but also for the longer and, in that respect, apparently more mature geometry of the fault system, as suggested by the negative exponential fault size distributions (Ackermann and Schlische, 1997).

Concerning the key-role played by transverse fault zones (N50°E and N140°E) on the KSFB development, the significance of earlier transverse structures is supported by the presence of cross-cutting, and possibly also contemporaneous faults, which parallel the N50°E and N140°E-oriented discontinuities bounding the KSFB to the north and south. The NW–SE fault trend is known to follow the trace of the Anza Cretaceous–Palaeogene rift (Greene et al., 1991; Bosworth, 1992; Smith and Mosley, 1993; Bosworth and Morley, 1994; Dindi, 1994; Ring, 1994; Morley et al., 1999b; Vétel and Le Gall, in press). Furthermore, it is well established that the Chew Bahir graben to the north had a protracted history of rifting prior to the deposition of the Gombe lavas. Combined with the uplifted nature of the Kino Sogo area and the presence of the westward downthrowing Fab fault, it is clear that, at some stage, the Buluk transverse zone must have transferred strain associated with the Chew Bahir graben westward into the Lake Turkana rift (Vétel and Le Gall, in press). The co-linearity of the KSFB and the Chew Bahir graben indicates that for some time during the past 3 Ma, a through-going 40-km-wide rift extended directly southwards possibly extending as far south as the Suguta Valley (Fig. 12b), a situation that may also have prevailed at some earlier time. Why such a radical change in rift geometry should occur is unknown, though it presumably reflects some diminution, however temporary, of the influence of the BTFZ. Moreover, the KSFB is transected by a N140°E-trending transverse central zone across which displacement is transferred southwards to an increased number of horst–graben pairs. The orientation of this zone, parallel to that of the pre-existing Cretaceous Anza rift, perhaps reflects an associated change in crustal structure, the nature of which is unknown. Other similarly oriented transverse faults to the south, together with those within the BTFZ, attest to the continued influence of long-lived transverse structures on rift fault geometry.

7. Conclusions

The KSFB is a 40-km-wide arcuate zone cutting through a thin (<200 m) Pliocene lava sequence on the eastern part of the broad Turkana rift zone (~200 km wide). Prior to the recent KSFB rifting event (<3.0 Ma), the early geometry of the Kino Sogo volcanic rifted area was defined by an asymmetrical uplifted fault block, tilted to the E–SE, and bounded by transverse discontinuities to the north (N50°E Buluk fault) and south (N140°E Anza-type structures). The present-day internal organisation of the KSFB is dominated by a regular horst and graben system with no dominant structures and with along-strike variations in structural style (density, direction and linkage of faults) suggesting the existence of three sub-segments separated by two NW–SE transverse fault zones. The fault system accommodates very low strains (<1%) and since it is no older than 3 Ma, it could be characterised by extension rates and strain rates that are as low as ~0.1 mm/yr and 10^{-16} s^{-1}, respectively. Fault scaling properties, such as fault length distributions, define negative exponential distributions, as opposed to the power-law scaling typical of other fault systems. Other unusual features of the system include the highly segmented characteristics of the system and the under-displaced nature of the faults, which show displacement/length scaling properties that lie outside of the field generally defined by faults. The scaling properties of the KSFB are most easily reconciled with an alternative model for fault growth (Walsh et al., 2002) in which fault lengths are established

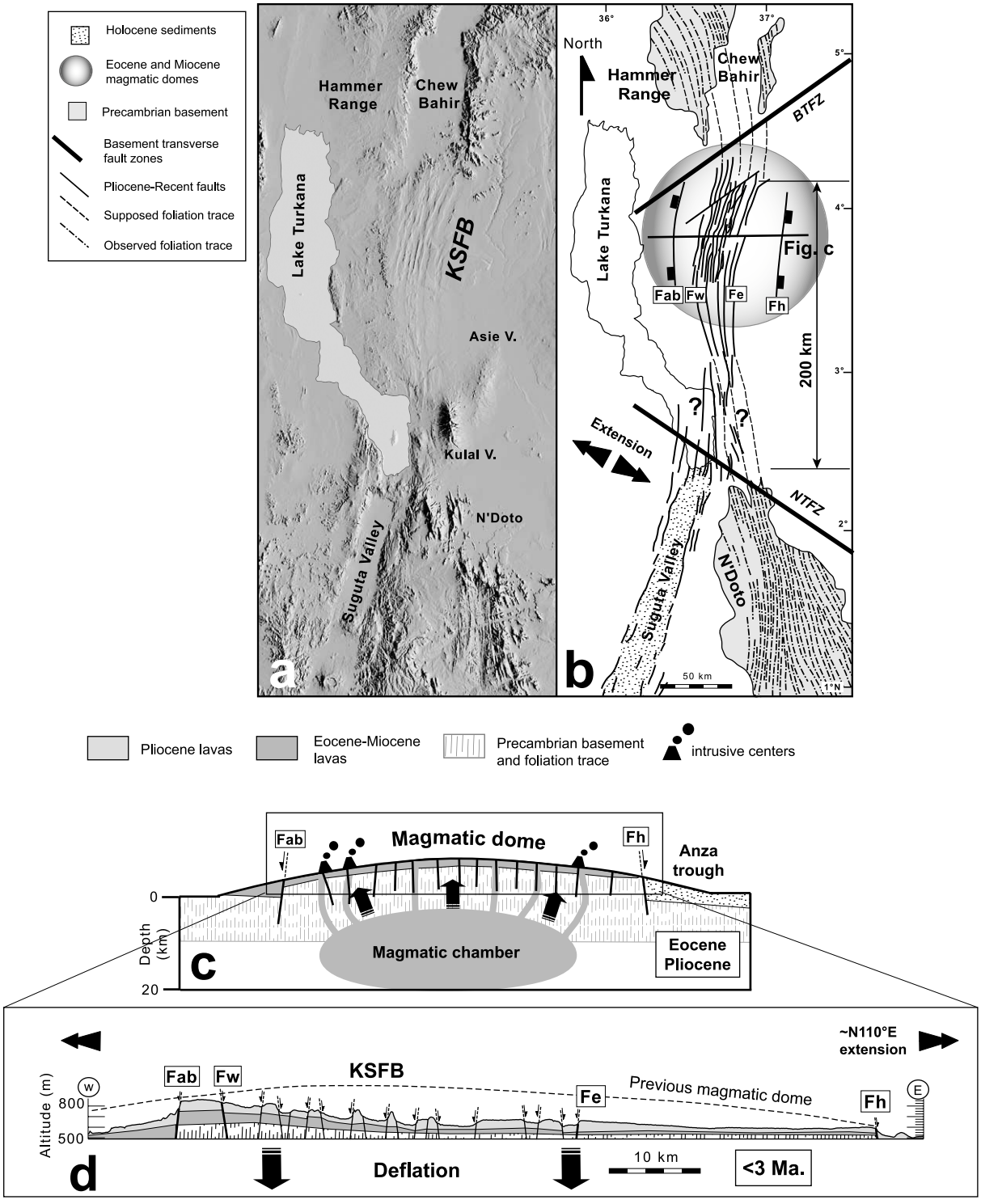

Fig. 12. Pre-existing structures that would have been susceptible to reactivation during the formation of the Kino Sogo Fault Belt (KSFB). (a) and (b) SRTM elevation data showing that the KSFB could represent a continuation of the sinusoidal trace of ductile/brittle structures in the N'Doto and Hammer Range basement massif or could link the Chew Bahir and Suguta Valley graben. These fabrics/structures appear to be dissected by two major transverse fault zones, the so-called N'Doto TFZ (NTFZ N140°E) and Buluk TFZ (BTFZ N50°E). (c) and (d) The Kino Sogo area is believed to be located over an earlier Eocene–Miocene and Pliocene magmatic thermal dome which may have lead to the formation of flexure-related faults/fractures at the top of the magmatic flexure, the orientation of which would have been controlled, to some extent, by the background rift-related WNW–ESE extension. (d) Cross-section of the top of the earlier formed magmatic dome. The KSFB may have formed by reactivation of pre-existing dome-related fractures (see Fig. 12b for location).

rapidly in response to the reactivation of inherited underlying structures. The potential controls on structural inheritance for the KSFB are the reactivation of underlying Proterozoic ductile fabrics or basement faults, with the latter possibly arising from Cenozoic rifting with or without the effects of volcanic doming. Combined with the structural controls exercised by earlier transverse structures, the KSFB demonstrates the strong influence of pre-existing structure on fault system growth and the relatively rapid development of under-displaced fault geometries at low strains.

Acknowledgements

Financial support was provided by the ECLIPSE (Environnements et Climats du passé) Program of INSU-CNRS, as well as by grants from SUCRI-2E and UMR CNRS 6538 "Domaines Océaniques". We thank Nancye Dawers for her helpful and constructive comments that improved the paper and members of the Fault Analysis Group for useful discussions. This publication is contribution no. 958 of the IUEM, European Institute for Marine Studies (Brest, France).

References

Ackermann, R.V., Schlische, R.W., 1997. Anticlustering of small normal faults around larger faults. Geology 25, 1127–1130.

Ackermann, R.V., Schlische, R.W., Withjack, M.O., 2001. The geometric and statistical evolution of normal fault systems: an experimental study of the effects of mechanical layer thickness on scaling laws. Journal of Structural Geology 23, 1803–1819.

Bosworth, W., 1992. Mesozoic and early Tertiary rift tectonics in East Africa. Tectonophysics 209, 115–137.

Bosworth, W., Maurin, A., 1993. Structure, geochronology and tectonic significance of the northern Suguta Valley (Gregory Rift), Kenya. Journal of the Geological Society, London 150, 751–762.

Bosworth, W., Morley, C.K., 1994. Structural and stratigraphic evolution of the Anza rift, Kenya. Tectonophysics 236, 93–115.

Cardon, H., 1999. Mécanisme de propagation des réseaux de failles: l'exemple du Rift Gregory (Kenya). Unpublished PhD thesis, University Claude Bernard, Lyon.

Cartwright, J.A., Mansfield, C., Trudgill, B., 1995. The growth of faults by segment linkage: evidence from the Canyonlands grabens of S.E. Utah. Journal of Structural Geology 17, 1319–1326.

Charsley, T.J., 1987. Geology of North Horr Area. Ministry of Environment and Natural Resources, Mines and Geology Department, Republic of Kenya. 40pp.

Childs, C., Walsh, J.J., Watterson, J., 1990. A method for estimation of the density of fault displacements below the limit of seismic resolution in reservoir formations. In: Buller, A.T., Berg, E., Hjelmeland, O., Kleppe, J., Torsaeter, O., Aasen, J.O. (Eds.), North Sea Oil and Gas Reservoir II. The Norwegian Institute of Technology. Graham and Trotman, London, pp. 309–318.

Cladouhos, T.T., Marrett, R., 1996. Are fault growth and linkage consistent with power-law distributions of fault lengths? Journal of Structural Geology 18, 281–293.

Cowie, P.A., Scholz, C.H., 1992. Displacement–length scaling relationship for faults: data synthesis and discussion. Journal of Structural Geology 14 (10), 1149–1156.

Cowie, P.A., Sornette, D., Vanneste, C., 1995. Multifractal scaling properties of a growing fault population. Geophysical Journal International 122, 457–469.

Dawers, N.H., Anders, M.H., Scholz, C.H., 1993. Fault length and displacement: scaling laws. Geology 21, 1107–1110.

Dindi, E.W., 1994. Crustal structure of the Anza graben from gravity and magnetic investigations. Tectonophysics 236, 359–371.

Dunkelman, T.J., Karson, J.A., Rosendahl, B.R., 1988. Structural style of the Turkana Rift, Kenya. Geology 16, 258–261.

Dunkelman, T.J., Rosendahl, B.R., Karson, J.A., 1989. Structure and stratigraphy of the Turkana rift from seismic reflection data. Journal of African Earth Science 8, 489–510.

Dunkley, P.N., Smith, M., Allen, D.J., Darling, W.G., 1993. The geothermal activity and geology of the northern sector of the Kenya Rift Valley. From Research Report SC/93/1, British Geological Survey for Kenyan Ministry of Energy, 183pp.

Ebinger, C.J., Yemane, T., Woldegabriel, G., Aronson, J.L., Walter, R.C., 1993. Late Eocene–Recent volcanism and faulting in the southern main Ethiopian rift. Journal of the Geological Society, London 150, 99–108.

Ebinger, C.J., Yemane, T., Harding, D.J., Tesfaye, S., Kelley, S., Rex, D.C., 2000. Rift deflection, migration and propagation: Linkage of the Ethiopian and Eastern rifts, Africa. GSA Bulletin 112, 163–176.

Feibel, C.S., Brown, F.H., McDougall, I., 1989. Stratigraphic context of fossil Hominids from the Omo Group deposits: Northern Turkana basin, Kenya and Ethiopia. American Journal of Physical Anthropology 78, 595–622.

Gabriel, G.W., Aronson, J.L., 1987. Chow Bahir rift: a 'failed' rift in southern Ethiopia. Geology 15, 430–433.

Gillespie, P.A., Walsh, J.J., Watterson, J., 1992. Limitations of dimension and displacement data from single faults and the consequences for data analysis and interpretation. Journal of Structural Geology 14, 1157–1172.

Girard, C.M., Girard, M.C., 1999. Traitement des données de Télédétection, Dunod, 528pp.

Gloaguen, R., 2000. Analyse quantitative de l'extension continentale par imagerie satellitale optique et radar. Application au rift sud-kenyan. Unpublished PhD Thesis, University of Brest.

Greene, L.C., Richards, D.R., Johnson, R.A., 1991. Crustal structure and tectonic evolution of the Anza rift, northern Kenya. Tectonophysics 197, 203–211.

Gupta, A., Scholz, C., 2000. Brittle strain regime transition in the Afar depression: implications for fault growth and seafloor spreading. Geology 28 (12), 1087–1090.

Hackman, B.D., Charsley, T.J., Key, R.M., Wilkinson, A.F., 1990. The development of the East African Rift system in north-central Kenya. Tectonophysics 184, 189–211.

Haileab, B., Brown, F.H., McDougall, I., Gathogo, P.N., 2004. Gombe Group basalts and initiation of Pliocene deposition in the Turkana depression, northern Kenya and southern Ethiopia. Geological Magazine 141 (1), 41–53.

Hendrie, D.B., Kusnir, N.J., Morley, C.K., Ebinger, C.J., 1994. Cenozoic extension in northern Kenya: a quantitative model of rift basin development in the Turkana region. Tectonophysics 236, 409–438.

Hetzel, R., Strecker, M.R., 1994. Late mozambique belt structures in western Kenya and their influence on the evolution of the Cenozoic Kenya Rift. Journal of Structural Geology 16 (2), 189–201.

Imber, J., Tuckwell, G.W., Childs, C., Walsh, J.J., Manzocchi, T., Heath, A.E., Bonson, C.G., Strand, J., 2004. Three-dimensional distinct element modelling of relay growth and breaching along normal faults. Journal of Structural Geology 26, 1897–1911.

Key, R.M., Watkins, R.T., 1988. Geology of the Sabarei area. Report 111, Ministry of Environment and Natural Resources, Mines and Geology Department, Ministry of Kenya, 57pp.

Kusznir, N.J., Marsden, G., Egan, S.S., 1991. A flexural cantilever simple-shear/pure shear model of continetal lithosphere extension: application to the Jeanne d'Arc Basin, Grand Banks and Viking Graben, North Sea.

In: Roberts, A.M., Yielding, G., Freeman, B. (Eds.), The Geometry of Normal Faults Special Publication Geological Society, London 56, pp. 41–60.

Le Turdu, C., 1998. Modèles tectono-sédimentaires 3D des bassins en extension. Exemples du Rift du Kenya (Baringo-Bogoria et Magadi), du Rift Ethiopien (Ziway-Shala) et du Fossé Nord-Tanganyika. Unpublished PhD Thesis, University of Brest, 416pp.

Main, J., 1996. Statistical physics, seismogenesis and seismic hazard. Reviews of Geophysics 34, 433–462.

Maurin, J.C., Guiraud, R., 1993. Basement control in the development of the Early Cretaceous West and Central African Rift System. Tectonophysics 228, 81–95.

Morley, C.K., Wescott, W.A., Harper, R.M., Wigger, S.T., Day, R.A., Karanja, F.M., 1999a. Geology and geophysics of the Western Turkana Basins. In: Morley, C.K. (Ed.), Geoscience of Rift Systems—Evolution of East Africa AAPG Studies in Geology, vol. 44, pp. 19–54.

Morley, C.K., Day, R.A., Lauck, R., Bosher, R., Stone, D.M., Wigger, S.T., Wescott, W.A., Haun, D., Bassett, N., Bosworth, W., 1999b. Geology and geophysics of the Anza Graben. In: Morley, C.K. (Ed.), Geoscience of Rift Systems—Evolution of East Africa AAPG Studies in Geology, vol. 44, pp. 67–90.

Nicol, A., Walsh, J.J., Watterson, J., Gillespie, P.A., 1996. Fault size distributions–are they really power-law? Journal of Structural Geology 18 (2/3), 191–197.

Ochieng', J.O., Wilkinson, A.F., Kagasi, J., Kimomo, S., 1988. Geology of the Loiyangalani Area. Ministry of Environment and Natural Resources, Mines and Geological Department, Republic of Kenya. 53pp.

Peacock, D.C.P., Sanderson, D.J., 1991. Displacements, segment linkage and relay ramps in normal fault zones. Journal of Structural Geology 13, 721–733.

Ring, U., 1994. The influence of pre-existing structure on the evolution of the Cenozoic Malawi rift (East African rift system). Tectonics 13, 313–326.

Schlische, R.W., Young, S.S., Achermann, R.V., Gupta, A., 1996. Geometry and scaling relations of a population of very small rift-related normal faults. Geology 24, 683–686.

Scholz, C.H., Cowie, P.A., 1990. Determination of total strain from faulting using slip-measurements. Nature 346, 837–839.

Shackelton, R.M., 1993. Tectonics of the Mozambique Belt in East Africa. In: Richard, H.M., Alabaster, T., Harris, N.B.W., Neary, C.R. (Eds.), Magmatic Processes and Plate Tectonics Special Publication Geological Society, London, 76, pp. 345–362.

Smith, M., Mosley, P., 1993. Crustal heterogeneity and basement influence on the development of the Kenya Rift, East Africa. Tectonics 12, 591–606.

Spyropoulos, C., Scholz, C.H., Shaw, B.E., 2002. Transition regimes for growing crack populations. Physical Review E 65, 056106.

Vétel, W., Le Gall, B., in press. Dynamics of prolonged continental extension in magmatic rifts: the Turkana Rift case study. Journal of the Geological Society, London, in press.

Villemin, T., Sunwoo, C., 1987. Distribution logarithmique self-similaire des rejets et longueurs de failles: exemple du Bassin Houiller Lorrain. Compte Rendu de l'Académie Sciences, Paris, Série II 305, 1309–1312.

Walsh, J.J., Watterson, J., 1988. Analysis of the relationship between the displacements and dimensions of faults. Journal of Structural Geology 10, 239–247.

Walsh, J.J., Watterson, J., Yielding, G., 1991. The importance of small-scale faulting in regional extension. Nature 351, 391–393.

Walsh, J.J., Nicol, A., Childs, C., 2002. An alternative model for the growth of faults. Journal of Structural Geology 24, 1669–1675.

Walsh, J.J., Bailey, W.R., Childs, C., Nicol, A., Bonson, C.G., 2003. Formation of segmented normal faults: a 3-D perspective. Journal of Structural Geology 25, 1251–1262.

Watkins, R.T., 1986. Volcano-tectonic control on sedimentation in the Koobi Fora sedimentary basin, Lake Turkana. In: Frostick, L.E. et al. (Ed.), Sedimentation in the African Rifts Geological Special Publication, 25, pp. 85–95.

Wilkinson, A.F., 1988. Geology of the Allia Bay area. Report 109, Ministry of Environment and Natural Resources, Mines and Geological Department, Republic of Kenya, 54pp.

Wu, H., Pollard, D.D., 1995. An experimental study of the relationship between joint spacing and layer thickness. Journal of Structural Geology 17, 887–905.

Yielding, G., Needham, T., Jones, H., 1996. Sampling of fault populations using sub-surface data: a review. Journal of Structural Geology 18 (2/3), 135–146.